J Appl Electrochem (2012) 42:59–67
DOI 10.1007/s10800-011-0371-3

ORIGINAL PAPER

Electrooxidation of formic acid at platinum nanoclusters electrodeposited on PEDOT coated carbon paper electrode

Sthitaprajna Dash · S. Patra · N. Munichandraiah

Received: 27 August 2011 / Accepted: 16 November 2011 / Published online: 26 November 2011

Abstract Nanoclusters of Pt were electrochemically deposited on a conducting polymer, namely, poly(3,4-ethylenedioxythiophene) (PEDOT), which was also electrochemically deposited on carbon paper current collector. PEDOT facilitated uniform distribution of Pt nanoclusters, when compared with Pt electrodeposition on bare carbon paper substrate. Spectroscopy data indicated absence of any interaction between PEDOT and Pt. The electrochemically active surface area as measured from carbon monoxide adsorption followed by its oxidation was several times greater for Pt–PEDOT/C electrode in comparison with Pt/C electrode. The catalytic activity of Pt–PEDOT/C electrode for electrooxidation of formic acid was significantly greater than that of Pt/C electrode. Amperometry data suggested that the electrodes were stable for continuous oxidation of HCOOH.

Keywords Platinum nanoclusters · Poly(3,4-ethylenedioxythiophene) · Formic acid oxidation · Cyclic voltammetry · Amperometry

1 Introduction

Formic acid is an attractive anode material for fuel cells because it exists as a liquid like methanol at room temperature. When dissolved in water, HCOOH is relatively non-toxic and non-explosive. It is therefore safe and easy in handling, transportation and storage in comparison with the gaseous and liquid hydrogen and also methanol. Furthermore, Willsau and Heitbaum [1] reported that formic acid was oxidized at a less positive potential than methanol. Rhee et al. [2] reported that diffusion of formic acid through Nafion membrane was slower than that of methanol. Slow diffusion of HCOOH facilities low fuel cross over, thus it can be used at high concentrations. Owing to these advantages, a direct formic acid fuel cell (DFAFC) is attractive from application view point. For electrochemical oxidation of formic acid, single crystal as well as polycrystalline Pt, Rh, Pd and Au electrodes have been used as catalysts [3–11]. Among these catalysts, Pt exhibits the highest catalytic activity for electrooxidation of formic acid. Nano structured materials have high surface area and large pore size in comparison to the bulk materials [12]. In previous studies of metal nanoparticles catalysts, it has been found that electrocatalytic activity depends strongly on the particle dimensions and surface morphology because of the variation of the density of active sites such as steps, edges, kinks, etc. [13–15]. Pt nano particles have been used as effective electrocatalysts for the electrooxidation of formic acid because of their high surface area when compared with large particles [16–20]. Electrocrystallization is a simple and efficient method for preparation of nano structured metal particles. Wu et al. [21] reported that electrocatalytic efficiency of Pt nano particles also depends on the supporting matrix. Generally carbon and carbon-based materials are used for supporting catalyst particles [22–30]. A thin film of electronically conducting polymer (CP) acts as a good dispersing material for Pt nanoparticles [31–37]. CPs offer great advantages due to their high electronic conductivity and mechanical strength, as well as good adhesion to the substrate electrode. Several polymers such as polyaniline (PANI), ploypyrrole (PPy), polythiophene (PTh), poly(3,4-ethylenedioxythiophene) (PEDOT), etc., have been investigated as catalyst supports for formic acid oxidation [31–37]. Zhu et al. [31] prepared

S. Dash (✉) · S. Patra · N. Munichandraiah
Indian Institute of Science, Bangalore, Karnataka, India
e-mail: sthitaprajna@ipc.iisc.ernet.in

Pt modified PANI/multi walled carbon nano tube (MWCNT) electrode by electrochemical deposition. From cyclic voltammetry studies, they showed that Pt modified PANI/MWCNT composite had a high electrocatalytic activity and long term stability for formic acid oxidation. Gholamian and Contractor [32] studied the effect of preparation conditions of PANI on the dispersion of Pt particles. Del Valle et al. [33] prepared Pt and Pt–Pb particles on PTh, PPy, PANI films. Becerik and Kadigan [34] dispersed Pt particles on perchlorate doped PPy films. Selvaraj et al. [35] investigated Pt and Pt–Pd nano particles dispersed in PPy–MWCNT films. Schrebler et al. [36] studied Pt and Pt–Pb particles dispersed on PTh films. Kelaidopoulou et al. [37] studied Pt modified poly-(2-hydroxy-3-aminophenazine). PEDOT was employed as dispersion medium for Pt particles in only a few studies [38–40] and the electrodes were used for methanol oxidation studies.

From the above, it is understood that catalyst particles dispersed on a CP exhibit greater catalytic activity than the same material in the absence of CPs. However, there are no reports to the best of authors' knowledge on electrooxidation of HCOOH on nano dimensions of Pt dispersed on PEDOT. In the present study, nanoclusters of Pt are electrochemically deposited on PEDOT, which is also electrochemically prepared from its monomer. PEDOT is strongly adherent on the substrate. Additionally, the electrochemically deposited PEDOT is porous, which facilitates enhanced surface area and a high porosity for the subsequently deposited Pt nanoclusters. Due to the presence of PEDOT, the electrochemical deposition of Pt results in the formation of Pt nanoclusters, which are uniformly distributed. The experimental results reveal that the catalytic activity of Pt–PEDOT/C electrode is greater than that of Pt/C electrode for electrooxidation of formic acid.

2 Experimental

All chemicals, namely, 3,4-ethylenedioxythiophene (EDOT, Aldrich), H_2SO_4 (Merck), sodium dodecyl sulphate (SDS, Merck), HCOOH (Merck) and chloroplatinic acid (Kemie) were used as received. All aqueous solutions were prepared in doubly distilled water. A Toray carbon paper (thickness: 0.2 mm) was used as the substrate for electrodeposition of PEDOT and Pt. A foil of 7 mm width and 3 cm length was sectioned out of a carbon sheet, 1.4 cm^2 area (geometric) at one end was exposed to the electrolyte and the rest of its length was used for electrical contact through a Cu wire. The unexposed area was masked by a PTFE tape to ensure that the electrolyte contacts only the required area. For PEDOT deposition, an electrolyte of 0.01 M EDOT + 0.01 M SDS + 0.1 M H_2SO_4 was used and electrodeposition on the carbon paper substrate was carried out at 0.9 V [41]. The charge was used as a measure to estimate the quantity of PEDOT deposited on carbon substrate. For all experiments, PEDOT was prepared by passing a charge of 70 mC cm^{-2}. After electrochemical deposition, PEDOT coated carbon paper electrode was washed repeatedly in a 0.1 M H_2SO_4 solution and then dried at 60 °C. For Pt deposition, 0.005 M H_2PtCl_6 + 0.1 M H_2SO_4 electrolyte was used and the deposition was carried out at 0.1 V. The deposition of Pt was carried out with two different charges: 70 and 350 mC cm^{-2}. By using these charges, the quantities of Pt were estimated as 0.036 and 0.18 mg cm^{-2}, respectively. Pt nanoparticles were deposited on PEDOT coated carbon paper as well as bare carbon paper (without PEDOT) for studies of comparison. A glass cell of 50 mL capacity with suitable ground glass joints was used for electrochemical studies. Pt foil auxiliary electrodes and saturated calomel reference electrode (SCE) was used for both electrodeposition and electrochemical characterization studies. Potential values are reported against SCE. All experiments were conducted in an air conditioned room 22 ± 1 °C. Potentiostatic deposition of PEDOT and Pt was carried out using Solatron electrochemical interface model SI 1287. IR spectra were recorded using Perkin Elmer Lambda 35 spectroscope. Raman spectra were recorded using Bruker RFS100/S spectroscope. Microscopy characterization was carried out by using FEI Company scanning electron microscope (SEM) model Sirion and transmission electron microscopy HRTEM model TECNAIF30. For TEM studies, carbon paper coated electrode was sonicated in acetone to disperse the coated materials. A few drops of acetone containing the dispersed material was dropped on carbon coated Cu grid for recording TEM images. Electrochemical experiments were carried out using Ecochemie and Solatron potentiostats models Autolab and SI1287, respectively.

3 Results and discussion

It was known that polymerization of EDOT to PEDOT could take place in non-aqueous media because of sufficient solubility of the monomer [42]. Recently, it was shown that the solubility of EDOT in aqueous acidic media also increased in the presence of surfactant, namely, SDS, and that EDOT could be polymerized to PEDOT by electrochemical routes [43]. EDOT undergoes electrochemical oxidation in acidic electrolytes, resulting in the deposition of PEDOT on the substrate (reaction 1).

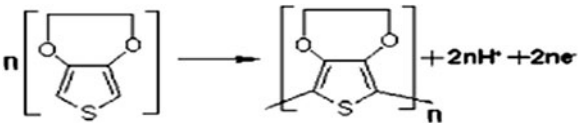

(1)

A carbon paper substrate was cycled in 0.01 M EDOT + 0.01 M SDS + 0.1 M H_2SO_4 electrolyte between 0 to 1.2 V, and the corresponding voltammogram is shown in Fig. 1a (curve (i)). Negligibly small current flows between 0.0 and 0.8 V in the forward sweep, suggesting the absence of any reaction in this potential region. There is an increase in current at 0.8 V resulting in a broad peak at 0.95 V. When a carbon paper electrode was cycled in 0.1 M H_2SO_4 + 0.01 M SDS (in the absence of EDOT), current peak at 0.95 V is absent (Fig. 1a, curve (ii)). The current peak in Fig. 1a (curve (i)) is thus due to the oxidation of EDOT to PEDOT on carbon paper. However, if the potential limit was increased to 1.5 V, two current peaks were observed (Fig. 1b). While the peak at 0.9 V is due to the oxidation of EDOT to PEDOT and the current peak appearing at 1.4 V is attributed to over-oxidation of PEDOT. The absence of any current peak in the reverse sweep suggests that the reactions occurring during the forward sweep are irreversible in nature, and that there are no reduction reactions in the potential range between 1.5 and 0.0 V. The potential of 0.9 V was chosen for PEDOT deposition without over-oxidation in the present work. The quantity of PEDOT deposited was estimated from the charge. The value of charge used for deposition was 70 mC cm^{-2} (geometric area) and this value corresponded to PEDOT mass of 53 μg cm^{-2} (geometric area). PEDOT coated carbon paper electrodes were subjected to SEM, IR and Raman spectroscopy. SEM image (Fig. 2a) shows that the substrate carbon paper is coated with PEDOT uniformly and that the coating is porous. The IR band (Fig. 2b, curve (i)) at 1,306 cm^{-1} is assigned to C–C or C=C stretching of thiophene ring [44]. The bands observed at 1171, 1140 and 1080 cm^{-1} are attributed to C–S bond stretching in thiophene ring. The peak corresponding to ring stretching is observed at 1,512 cm^{-1}. In Raman spectrum of PEDOT (Fig. 2c, curve (i)), one strong peak at 1,424 cm^{-1} and few weaker bands are present [45]. Raman spectrum (Fig. 2c) is similar to that reported for PEDOT prepared by a chemical route [45]. Pt nanoclusters were deposited on PEDOT coated carbon paper. IR spectrum as well as Raman spectrum of Pt modified PEDOT coated carbon electrode (Fig. 2b, c) are very similar to those of PEDOT (without any new bands or shift in the position of existing bands), indicating the absence of any chemical interaction between Pt and PEDOT. This also suggests that the polymer composition or structure is not affected by electrodeposited Pt particles.

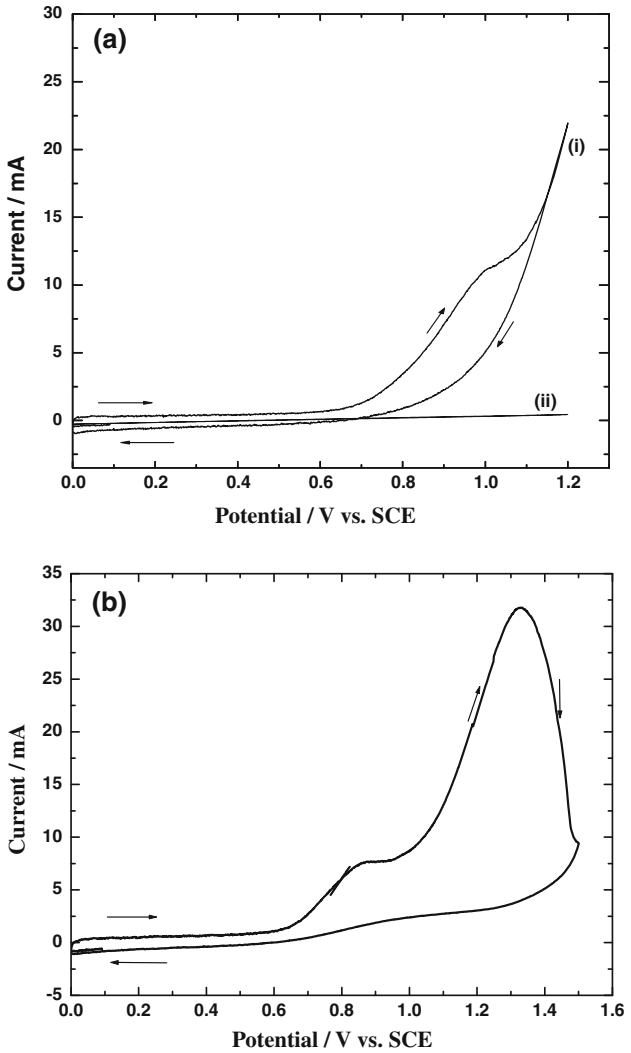

Fig. 1 **a** Cyclic voltammograms of carbon paper electrodes in 0.01 M EDOT + 0.01 M SDS + 0.1 M H_2SO_4 (*curve (i)*) and in 0.01 M SDS + 0.1 M H_2SO_4 (*curve (ii)*) between 0 and 1.20 V at 10 mV s^{-1}. **b** Cyclic voltammogram of carbon paper electrode in 0.01 M EDOT + 0.01 M SDS + 0.1 M H_2SO_4 at 10 mV s^{-1} between 0 and 1.50 V. Geometric area of the electrode: 1.4 cm^{-2}

SEM micrographs of Pt deposited on carbon paper with and without PEDOT under-layer are shown in Fig. 3 for the purpose of comparison. The quantity of charge passed for the deposition of Pt on both electrodes was the same (70 mC cm^{-2} (geometric)). It is seen that the distribution of Pt clusters is uniform on PEDOT covered carbon paper (Fig. 3a). The size of clusters range from 10 to 100 nm. As discussed later, the clusters are composed of Pt nanoparticles. In the absence of PEDOT on the carbon paper substrate, the Pt clusters grow larger in size (Fig. 3b) and they are distributed non-uniformly. SEM micrographs of Pt–PEDOT/C and Pt/C electrodes prepared with 350 mC cm^{-2} (geometric) charge for Pt deposition are

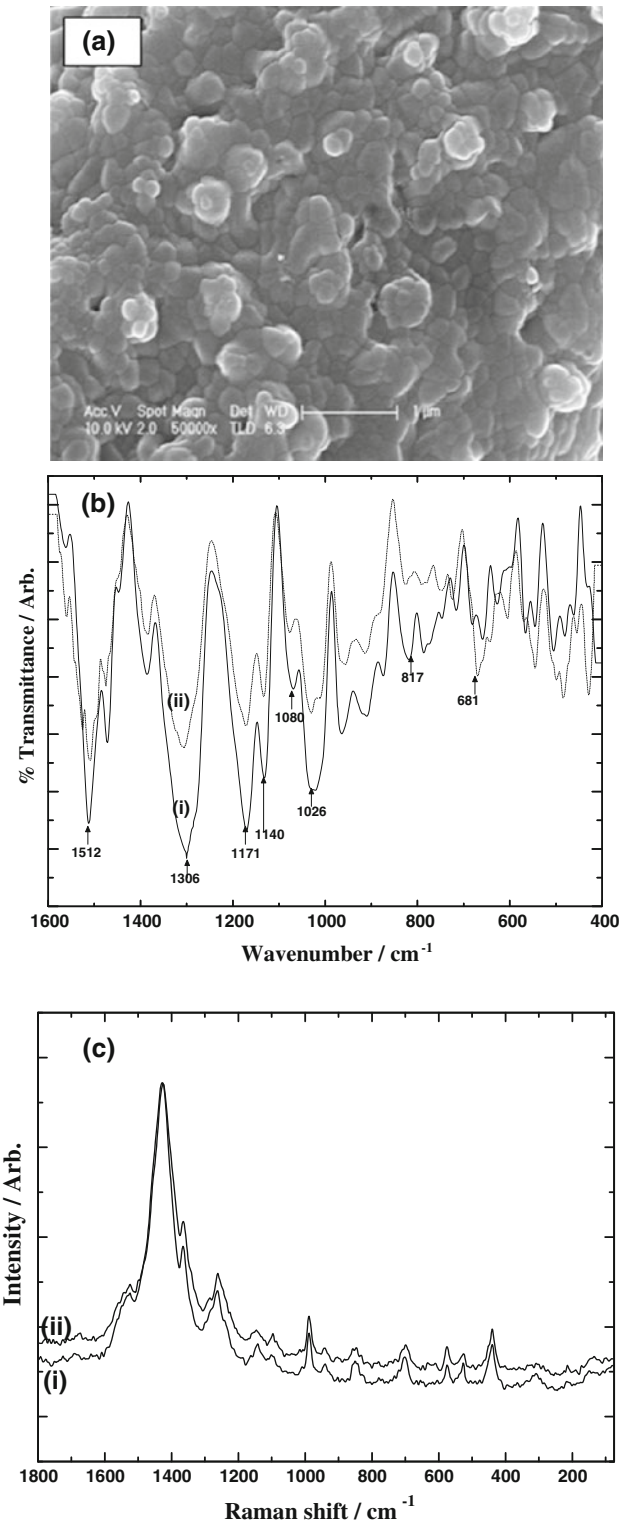

Fig. 2 **a** SEM micrograph of PEDOT coated carbon paper, **b** IR spectra of PEDOT (*curve (i)*) and Pt–PEDOT (*curve (ii)*) and **c** Raman spectra of PEDOT (*curve i*) and Pt–PEDOT (*curve (ii)*)

shown in Fig. 4. Similar to the observation made from Fig. 3, small Pt clusters are uniformly distributed on PEDOT covered carbon paper (Fig. 4a), whereas larger

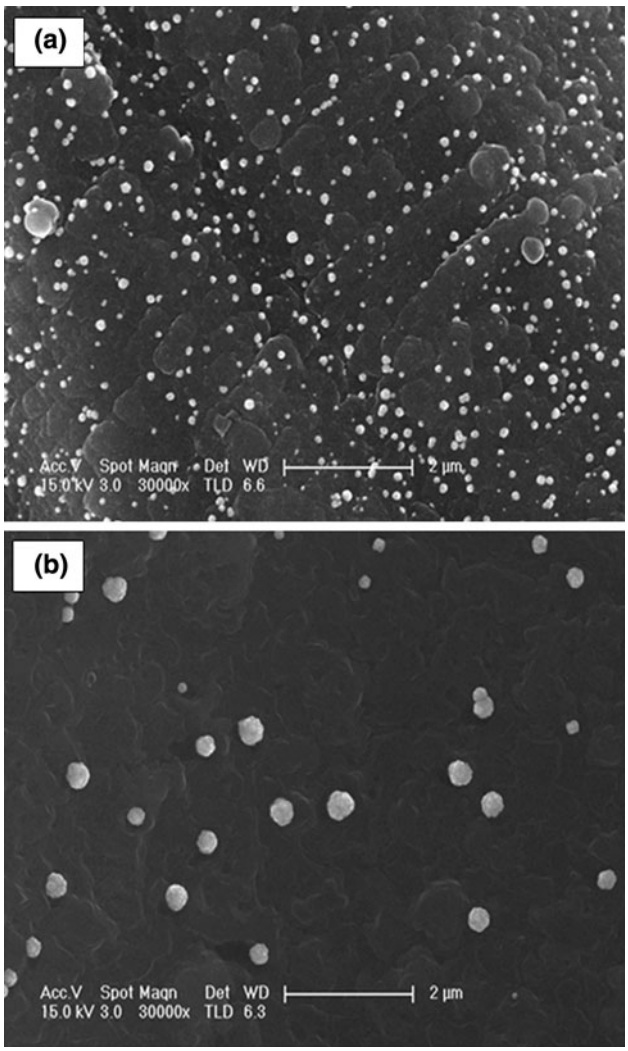

Fig. 3 SEM micrographs of **a** Pt–PEDOT coated carbon paper electrode and **b** Pt coated carbon paper electrode (Pt deposition charge: 70 mC cm^{-2} (geometric area))

clusters are non-uniformly present on bare carbon paper (Fig. 4b). The micrographs presented in Figs. 3 and 4 suggest that the layer of PEDOT present on carbon paper allows the electrocrystallization of Pt uniformly on the surface. The size of the Pt clusters is in the range of 10–100 nm in Fig. 3a for Pt deposited with 70 mC cm^{-2} (geometric) charge. On increasing the deposition charge to 350 mC cm^{-2} (geometric), Pt clusters grow in size (Fig. 4a) to 200–400 nm. It was also observed that if Pt was deposited with higher charge (>1 C cm^{-2}), the clusters merged and appearance of a film of Pt on the carbon paper substrate was noticed (SEM micrograph not shown). Thus, it is understood that the layer of PEDOT facilitates the electrodeposition of homogenously distributed small clusters of Pt. Electrocrystallization is the first step in the process of electrodeposition of metals or metal oxides. High energy surface sites such as crystal edges, kinks,

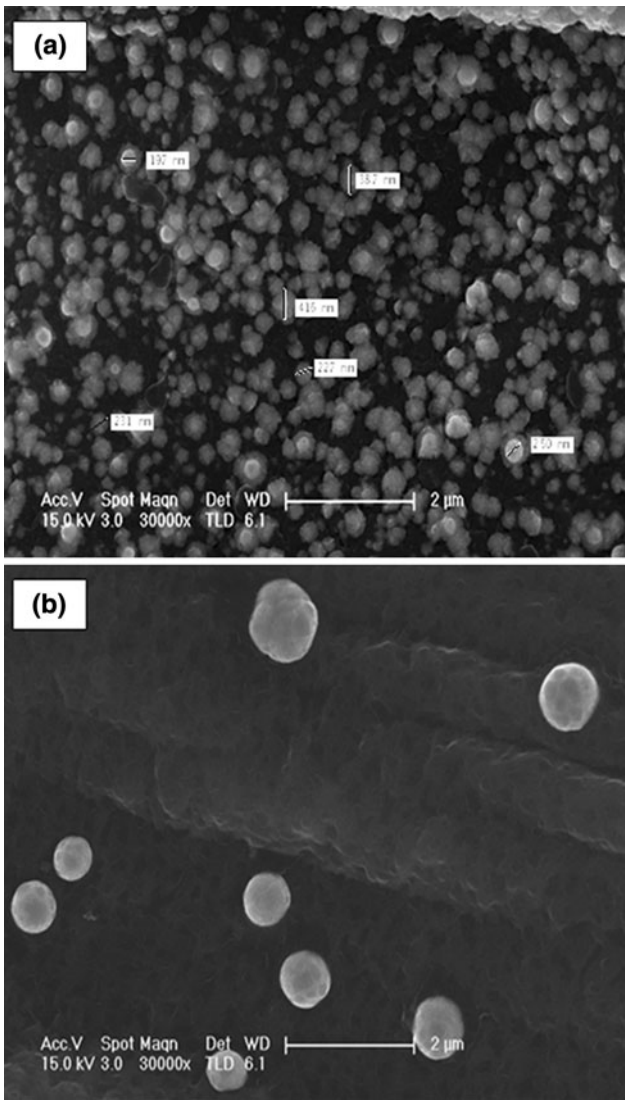

Fig. 4 SEM micrographs of **a** Pt–PEDOT coated carbon paper electrode and **b** Pt coated carbon paper electrode (Pt deposition charge: 350 mC cm^{-2} (geometric area))

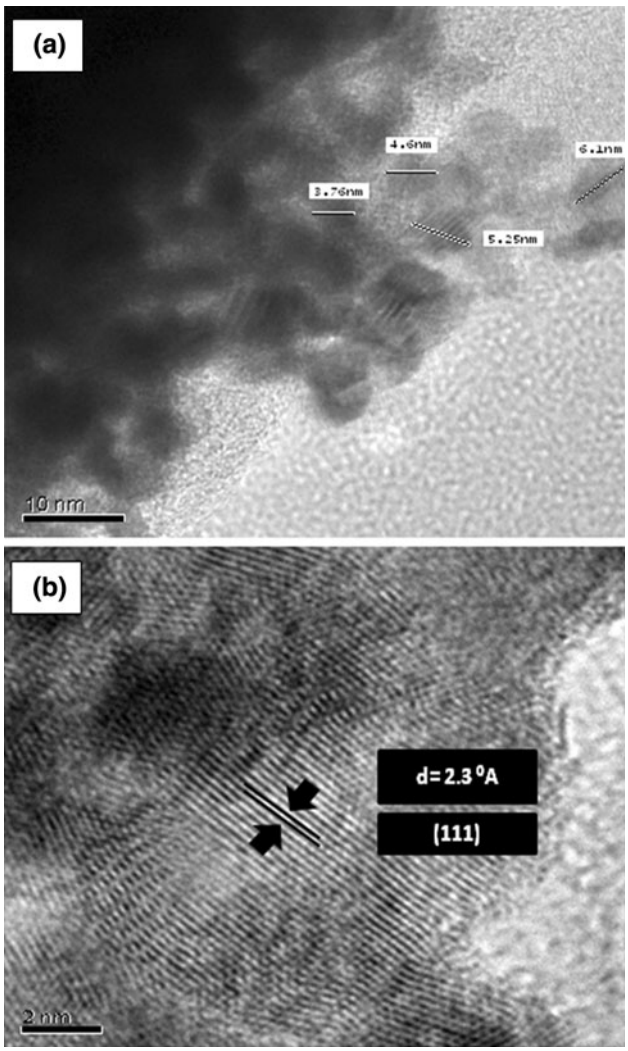

Fig. 5 **a** TEM image, and **b** HRTEM image of Pt–PEDOT/C electrode (Pt deposition charge: 350 mC cm^{-2} (geometric area))

steps, corners, defects, etc., present on the substrate favour electrocrystallization. It is likely that the electrodeposited PEDOT possesses a uniformly distribute, large number of surface defects. These defects are the sites for initiation of electrocrystallization of Pt nuclei and their further growth. TEM micrographs of a Pt cluster (350 mC cm^{-2} (geometric)) deposited on PEDOT covered carbon paper are shown in Fig. 5. It is seen that a cluster consists of nanoparticles of less than 10 nm size (Fig. 5a). The value of lattice spacing 2.3 Å measured in HRTEM image (Fig. 5b) corresponds to (111) plane of the Pt crystal.

The electrochemically active surface area of electrodeposited Pt agglomerates was evaluated by CO adsorption followed by electrooxidation method. For this purpose, a Pt coated electrode (Pt–PEDOT/C and Pt/C electrodes) was inserted into 0.5 M H_2SO_4 present in an air tight glass cell, and CO was bubbled for 30 min. Following this, the CO adsorbed Pt electrode was removed from the electrolyte, rinsed, transferred into another cell consisting of 0.5 M H_2SO_4 saturated with N_2 and subjected to cyclic voltammetry. Voltammogram of Pt–PEDOT/C electrode (Pt prepared with 70 mC cm^{-2} (geometric)) is typically shown in Fig. 6. A well defined peak corresponding to oxidation of CO (which is absent in the absence of CO adsorption) is present. Charge corresponding to the current peak is 10 mC for 1.4 cm^2 (geometric) electrode. Theoretically, CO oxidation charge is 420 µC for 1 cm^2 area of electrochemically active Pt [46]. Thus 10 mC corresponds to 23.94 cm^2 of Pt. The actual electrochemically active Pt surface is 17.1 cm^2 per 1 cm^2 geometric area of the electrode. Similarly, for Pt deposited with 70 mC cm^{-2} (geometric) on carbon paper in the absence of PEDOT, the electrochemically active Pt surface obtained is 1.9 cm^2 per 1 cm^2

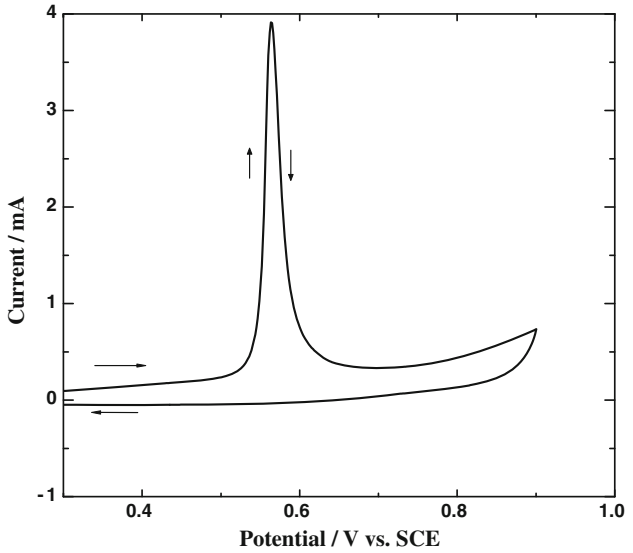

Fig. 6 CO anodic stripping voltammogram of Pt–PEDOT/C electrode (Pt deposition charge: 70 mC cm^{-2}). Geometric area of the electrode: 1.4 cm^{-2}

geometric area. Thus the roughness factors with respect to electrochemical activity for Pt–PEDOT/C and Pt/C electrodes are 17.1 and 1.9, respectively.

Cyclic voltammograms of Pt–PEDOT/C and Pt/C electrodes (both 70 mC cm^{-2}) recorded in 1 M HCOOH + 0.1 M H_2SO_4 are shown in Fig. 7a. In the forward sweep starting from 0 to 1.0 V, there are two anodic current peaks denoted as P_{f1} and P_{f2}, and there is another anodic current peak denoted as P_b in the reverse sweep. These three current peaks appear on both the electrodes. However, current of the voltammogram is greater for Pt–PEDOT/C electrode than for Pt/C electrode. As the electrodeposition of Pt was carried out with a charge of 70 mC cm^{-2} for both electrodes (Fig. 7a) and therefore the same amount of Pt (0.036 mg cm^{-2} (geometric) or 0.050 mg for the electrode of 1.4 cm^2 geometric) is present on both electrodes, the higher current density of Pt–PEDOT/C electrode than the Pt/C electrode is attributed to the greater dispersion of smaller nanoclusters of Pt on PEDOT.

The complete electrooxidation of HCOOH results in the formation of CO_2 as the final product (reaction 2).

$$HCOOH \rightarrow CO_2 + 2H^+ + 2e^- \quad (2)$$

There are two mechanisms, namely, direct path and indirect path mechanisms reported for the oxidation of HCOOH [4, 7]. In the direct path mechanism, the reaction is expected to proceed as written in Eq. 2 without involving any reaction intermediates. The current peak P_{f1} (Fig. 7a) is ascribed to the direct oxidation of HCOOH to CO_2. The indirect path mechanism involves the formation of CO or/and HCO as the reaction intermediate, in which C is attached to a site on the catalyst. The anodic current peak P_{f2} (Fig. 7a) is

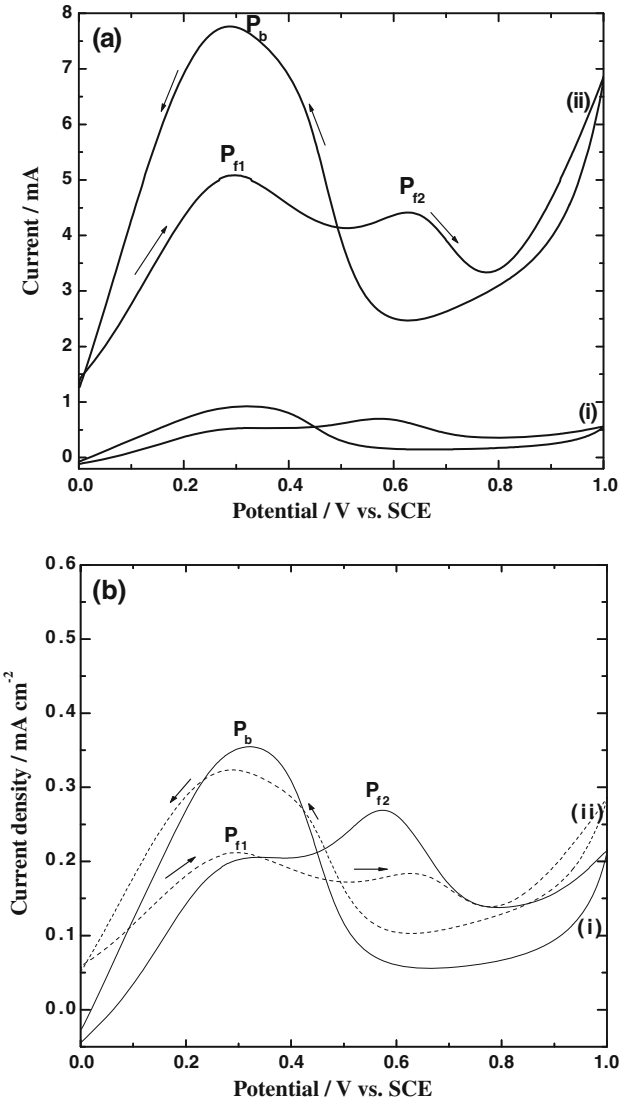

Fig. 7 **a** Cyclic voltammograms of (*i*) Pt/C and (*ii*) Pt–PEDOT/C electrodes (geometric area: 1.4 cm^{-2}) in 1 M HCOOH + 0.1 M H_2SO_4 at a sweep rate 20 mV s^{-1} (Pt deposition charge: 70 mC cm^{-2}). **b** Cyclic voltammograms presented in (**a**) are normalized to true area (obtained from CO oxidation) of Pt on Pt/C (*curve (i)*) and Pt–PEDOT/C (*curve (ii)*) electrodes

ascribed to the oxidation of the intermediates on Pt surface. The presence of P_b in the voltammogram (Fig. 7a) is also attributed to the direct oxidation of HCOOH to CO_2. It is interesting to note that the magnitude of currents for the three oxidation peaks is greater for Pt–PEDOT/C electrode than for Pt/C electrode, in spite of the fact that both electrodes contain the same quantity of Pt. This is due to fact that the Pt–PEDOT/C electrode consists of finer nanoclusters of Pt than the Pt/C electrode as evidenced from SEM micrographs (Fig. 3a, b). Furthermore, the ratio of peak currents of peaks P_{f1} (0.52 mA) and P_{f2} (0.81 mA) is 0.64 for Pt/C electrode (Fig. 7a, curve (i)), suggesting that the indirect path mechanism is predominant. On the other hand,

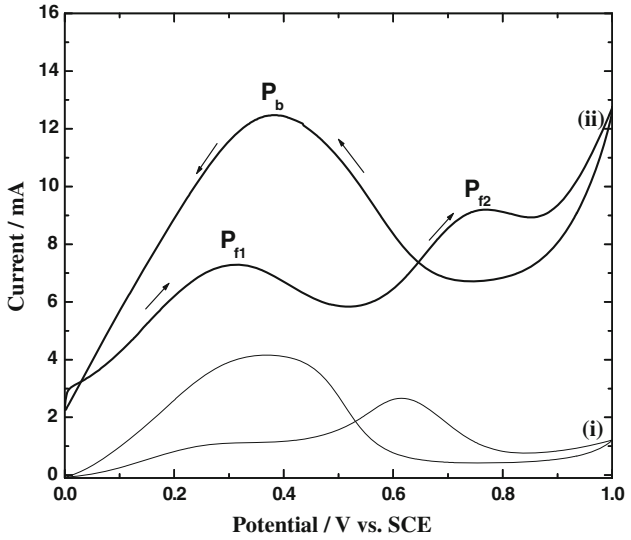

Fig. 8 Cyclic voltammograms of (*i*) Pt/C and (*ii*) Pt–PEDOT/C electrodes in 1 M HCOOH + 0.1 M H_2SO_4 at a sweep rate 20 mV s^{-1}. Pt deposition charge: 350 mC cm^{-2}; geometric electrode area: 1.4 cm^{-2}

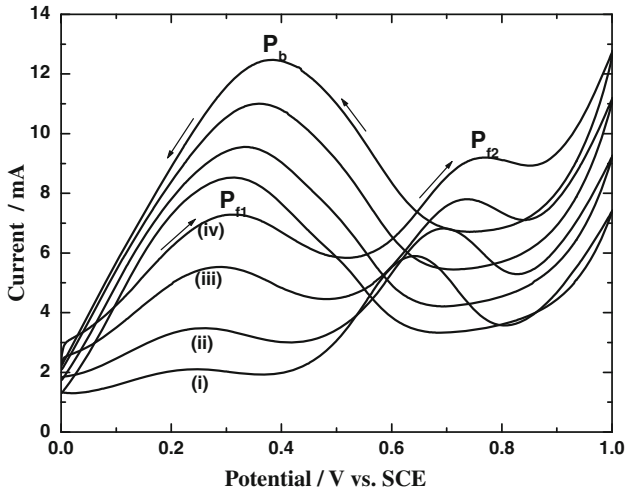

Fig. 9 Cyclic voltammograms of Pt–PEDOT/C electrode in 1.0 M HCOOH + 0.1 M H_2SO_4 at sweep rate of (*i*) 5, (*ii*) 10, (*iii*) 20, and (*iv*) 30 mV s^{-1}. Pt deposition charge: 350 mC cm^{-2}; geometric electrode area: 1.4 cm^{-2}

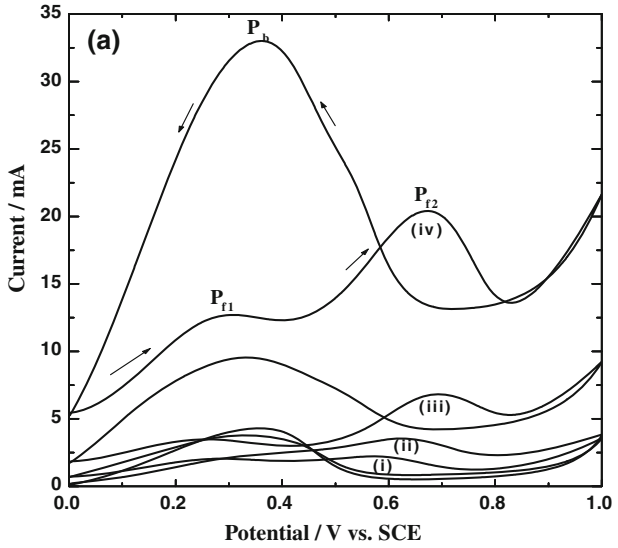

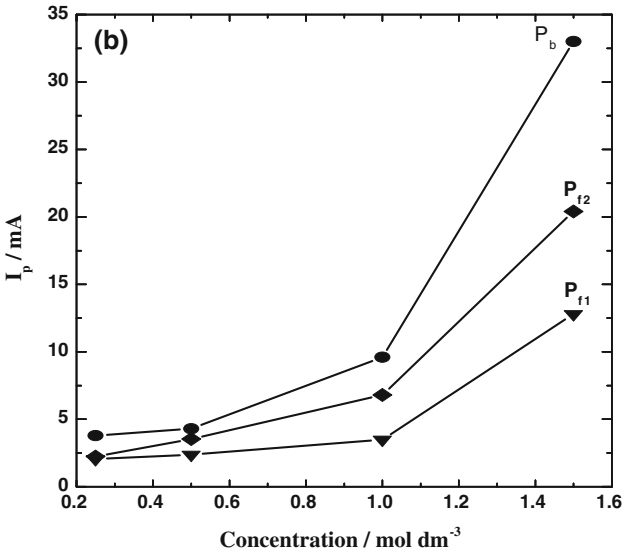

Fig. 10 a Cyclic voltammograms of Pt–PEDOT/C electrode in 0.1 M H_2SO_4 consisting of HCOOH at a concentration of (*i*) 0.25, (*ii*) 0.5, (*iii*) 1.0, and (*iv*) 1.5 M at a sweep rate of 20 mV s^{-1}. Geometric area of the electrode: 1.4 cm^{-2}; Pt deposition charge: 350 mC cm^{-2}. **b** Plots of peak currents versus concentrations

this ratio is 1.21 for Pt–PEDOT/C electrode. This indicates that the direct path mechanism is more dominant on Pt–PEDOT/C electrode. For the purpose of comparing Pt–PEDOT/C and Pt/C electrodes, the sum of peak currents of P_{f1} and P_b peaks (13 mA) for Pt–PEDOT/C electrode is greater than the same parameter (1.44 mA) for Pt/C electrode by about nine times. Thus for obtaining a peak current of 1.44 mA, the quantity of Pt required on Pt-PEDOT/C electrode can be decreased by about nine times. These observations clearly show the advantages of the PEDOT under-layer for the electrocatalytic activity of Pt for HCOOH oxidation. Using the real surface area values obtained from CO adsorption–oxidation studies, the voltammograms of Fig. 7a are re-plotted by normalizing the current per unit real area, and shown in Fig. 7b. It is seen that the voltammograms of both Pt–PEDOT/C and Pt/C electrodes nearly overlay each other. This suggests that the difference between voltammograms of these electrodes observed in Fig. 7a is entirely due to the difference in real surface of the electrodeposited Pt.

Similar to the above, cyclic voltammograms of 350 mC cm^{-2} Pt deposited Pt/C and Pt–PEDOT/C electrodes are shown in Fig. 8. The currents of the three peaks are greater for Pt–PEDOT/C electrode than for Pt/C

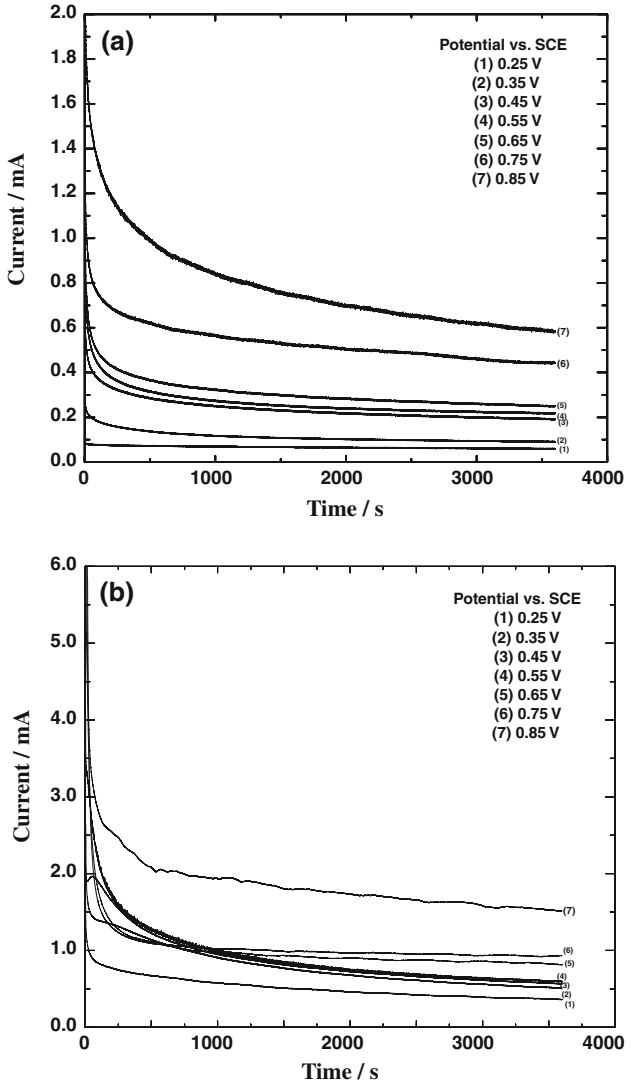

Fig. 11 Amperometry data at different potential values of **a** Pt–PEDOT/C (Pt deposition charge: 70 mC cm^{-2}) and **b** Pt–PEDOT/C (Pt deposition charge: 350 mC cm^{-2}) electrodes in 1.0 M HCOOH + 0.1 M H_2SO_4. Geometric area of the electrode: 1.4 cm^{-2}

electrode. The sum of peak currents of P_{f1} and P_b peaks (20 mA) for Pt–PEDOT/C electrode is greater than the same parameter (4.5 mA) for Pt/C electrode by about five times. It is thus reconfirmed that the presence of underlayer of PEDOT is an advantage in enhancing the catalytic activity of Pt towards oxidation of formic acid. Cyclic voltammograms of Pt–PEDOT/C (350 mC cm^{-2}) recorded at several sweep rates are shown in Fig. 9. There is an increase in size of the voltammogram with an increase in sweep rate. Cyclic voltammograms of Pt–PEDOT/C electrodes (350 mC cm^{-2}) recorded in 0.1 M H_2SO_4 consisting of different concentrations of HCOOH are presented in Fig. 10a. It is seen that the size of the voltammogram increases with an increase of concentration of HCOOH. The variations of peak currents with concentration of HCOOH are shown in Fig. 10b. The non-linearity of the data suggests the presence of adsorption effects on kinetics of the reactions. The data suggest that the Pt–PEDOT/C electrodes possess a high catalytic activity under various experimental conditions. The amperometry data of Pt–PEDOT/C electrodes recorded in stirred solution of 1 M HCOOH + 0.1 M H_2SO_4 at different potentials are shown in Fig. 11. After an initial decrease, currents are fairly constant over 1 h of the experiment conducted at each potential. These data suggest that the Pt–PEDOT/C electrodes possess stable electrochemical activity.

4 Conclusions

Electrooxidation of HCOOH was studied on Pt electrodeposited on PEDOT coated carbon paper substrate. PEDOT present on the substrate enhances the surface defects necessary for the electrocrystallization of Pt. Nanoclusters of Pt were uniformly distributed on PEDOT, whereas Pt deposited on bare carbon paper grew in large size. As a result, the electrochemically active surface of Pt was greater on PEDOT coated substrate than on the bare substrate. Cyclic voltammetry results showed that the Pt–PEDOT/C electrode was several times greater than Pt/C electrode. Both Pt–PEDOT/C and Pt/C electrodes were found stable for continuous electrolysis.

References

1. Willsau J, Heitbaum J (1986) Electrochim Acta 31:943
2. Rhee YW, Ha SY, Masel RI (2003) J Power Sources 117:35
3. Brummer SB (1965) J Phys Chem 69:1363
4. Capon A, Parasons R (1973) J Electroanal Chem 44:1
5. Capon A, Parasons R (1973) J Electroanal Chem 45:205
6. Capon A, Parasons R (1973) J Electroanal Chem 44:239
7. Wieckowski A, Sobkowski J (1975) J Electroanal Chem 63:365
8. Lamy C, Leger JM (1992) Proc Electrochem Soc 92:111
9. Wasmus S, Tryk DA, Vielstich W (1994) J Electroanal Chem 377:205
10. Lu GQ, Crown A, Wieckowski A (1999) J Phys Chem B 103:9700
11. Xu JB, Zhao TS, Liang ZX (2003) J Power Sources 185:857
12. Jing JY, Mehnert CP, Wong MS (1999) Angew Chem Int Ed 38:56
13. Zhou WP, Lewera A, Larsen R, Masel RI, Bagus PS, Wieckowski A (2006) J Phys Chem B 110:13393
14. Bergamaski K, Pinheiro ALN, Nart FC (2006) J Phys Chem B 110:19271
15. Mayrhofer KJJ, Blizanac BB, Arenz M, Ross PN, Markovic NM (2005) J Phys Chem B 109:14433
16. Wang Z, Qiu K (2006) Electrochem Commun 8:1071
17. Jiang JH, Kucernak A (2002) J Electroanal Chem 520:64
18. Yang H, Vante NA, Leger JM, Lamy C (2004) J Phys Chem B 108:1938
19. Chen W, Kim J, Sun S, Chen S (2007) Langmuir 23:11303

20. Waszczuk P, Banard TM, Rice C, Masel RI, Weickowski A (2002) J Electrochem Commun 4:599
21. Wu G, Chen YS, Xu BQ (2005) J Electrochem Commun 7:1237
22. Li H, Sun G, Jiang Q, Zhu M, Sun S, Xin Q (2007) J Electrochem Commun 9:1410
23. Li X, Hsing IM (2006) Electrochim Acta 51:3477
24. Liu Z, Hong L, Tham MP, Lim TH, Jiang H (2006) J Power Sources 161:831
25. Otomo J, Nishida S, Takahashi H, Nagamoto H (2008) J Electroanal Chem 615:84
26. Wang H, Jusys Z, Behm RJ (2004) J Phys Chem B 108:19413
27. Lee JS, Han KI, Park SO, Kim HN, Kim H (2004) Electrochim Acta 50:807
28. Uchida M, Aoyama Y, Tanabe M, Yanagihara N, Eda N, Ohta A (1995) J Electrochem Soc 142:2572
29. Raghuveer V, Manthiram A (2005) J Electrochem Soc 152: A1504
30. Patra S, Munichandraiah N (2008) Synth Met 158:430
31. Zhu ZZ, Wang Z, Li HL (2008) Appl Surf Sci 254:2934
32. Gholamian M, Contractor AQ (1990) J Electroanal Chem 289:69
33. Del Valle MA, Diaz FR, Bodini ME, Pizarro T, Cordova R, Gomez H, Schrebler R (1997) J Appl Electrochem 28:943
34. Becerik I, Kadigan F (2001) J Electrochem Soc 148(5):D49
35. Selvaraj V, Alagar M, Sathish Kumar K (2007) Appl Catal B 75:129
36. Schrebler R, Del Valle MA, Gomez H, Veas C, Cordova R (1995) J Electroanal Chem 380:219
37. Kelaidopoulou A, Abelidou E, Kokkinidis G (1999) J Appl Electrochem 29:1255
38. Kuo C-W, Huang L-M, Wen T-C, Gopalan A (2006) J Power Sources 160:65
39. Drillet J-F, Dittmeyer R, Juttner K (2007) J Appl Electrochem 37:1219
40. Patra S, Munichandraiah N (2009) Langmuir 25:1732
41. Patra S, Munichandraiah N (2007) J Appl Polym Sci 106:1160
42. Zhanga S, Houa J, Zhangc R, Xua J, Niea G, Pub S (2008) J Electroanal Chem 619:193
43. Honholz D, MacDiarmid AG, Saron DM Jr, Jones WE (2001) Chem Commun 23:2444
44. Feng W, Li Y, Wu J, Noda H, Fujii A, Ozaki M, Yoshino K (2007) J Phys Condens Matter 19:186220
45. Selvaganesh SV, Mathiyarasu J, Phani KLN, Yagnaraman V (2007) Nanoscale Res Lett 2:546
46. Brett DJL, Atkins S, Brandon NP, Vasileiadis N, Kucernak AR (2004) J Power Sources 133:205